VAWT: The virtual aerodynamic/aeroacoustic wind tunnel

GARY S. STRUMOLO
Scientific Research Laboratory, Ford Motor Company, P.O. Box 2053, Dearborn, MI 48121, U.S.A.

Abstract. Ever since computational fluid dynamics (CFD) arose as a tool for predicting fluid motions engineers have looked to the day when it could be used reliably to supplement wind tunnel tests. Limits on computer speed and algorithm accuracy have prevented the development of a virtual wind tunnel. But now, a team from Ford Research has developed the capability that allows engineers to evaluate vehicle designs both aerodynamically and aeroacoustically in a virtual environment. Starting with a CAD surface description of the vehicle, a CFD simulation can be constructed and executed with little user intervention in only a few days. This information can be used to estimate interior sound due to wind noise, which can then be played through speakers for a comparison of alternate vehicle designs. The technology that makes this possible combines a new method for CFD called PowerFlow^{TM} (from the Exa Corporation) with an enhanced *Wind Noise Modeller*$^{©}$. To illustrate this new capability, we will consider an analysis of the Taurus line. Aerodynamic information regarding flow around the side mirror and windshield wipers will be provided, and aeroacoustic wind-noise predictions will be made and compared to actual wind tunnel tests.

Key words: aeroacoustics, CAD (computer-aided design), CFD (computational fluid dynamics), SEA (statistical energy analysis), SPL (sound-pressure level), VAWT, WNM (wind-noise modeller).

1. Introduction

In recent years a relatively new approach to CFD, commonly referred to as the lattice gas method has emerged. The latest embodiment of this theory, commercialized by the Exa Corporation and called PowerFlow^{TM}, incorporates lattice gas principles to predict fluid motion. In this paper, we describe how this new technology has been combined with the patented Wind Noise Modeller$^{©}$ (US# 5,568,404, [1]) developed at Ford to create a *virtual aerodynamic/aeroacoustic wind tunnel*, or VAWT for short.

We will illustrate how the VAWT works by running through an investigation we conducted on the Ford Taurus. Our focus will be on two vehicle problems: wind noise and water flow up the windshield. We will demonstrate how the VAWT can be used to predict interior sound pressure levels at the driver's car, and compare our predictions to actual wind-tunnel measurements. We will do this by examining the effects of the A-pillar[1] and side mirror on side glass-flow patterns and pressure distributions. This information will be fed to the WNM for sound pressure level estimations and compared to measurements made in the Lockheed wind tunnel. Water flowing up the windshield from the wiper blade tips will also be examined with the VAWT and qualitatively compared to experiments.

---

[1]There are 3 'pillars' on a vehicle - labeled A, B, and C – between the roof and the car body. The A-pillar is the structural beam between the front windshield and the front side glass, the B-pillar is between the front and rear side windows, and the C-pillar is between the rear side window and the back window (either side).
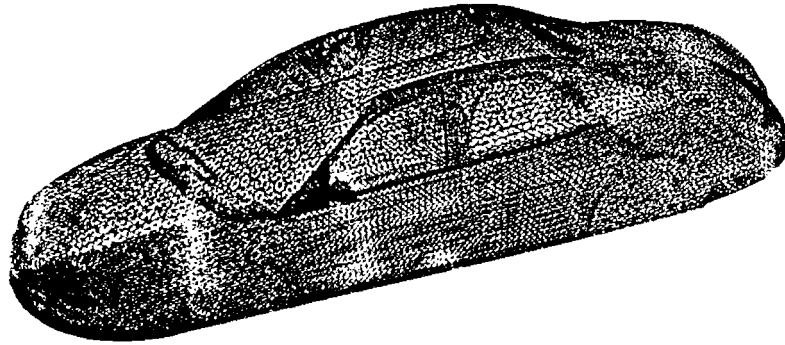
Figure 1. Taurus CAD surface model.

2. The VAWT

A CAD rendition of the vehicle surface is fed to the PowerFlow code, which automatically creates a computational mesh of it in a wind tunnel. The code then computes the transient flow over the vehicle, which we average over a suitable time interval to yield a 'pseudo-steady-state'. One of the outputs from this analysis is the flow detail over the side glass (A-pillar vortex location and strength, mirror wake details, pressure coefficient distribution). This information, in turn, is fed to the *Wind Noise Modeller*, which predicts the interior sound pressure level at the driver's ear due to wind noise. Finally, this spectral information is used to shape a white noise sound file and generate a representation of the wind noise, which is played through stereo speakers. The time from a valid surface file to hearing the wind noise sound is approximately 1 day on a 14-processor Sun E4000 workstation.

2.1. VEHICLE PREPARATION

Real wind tunnel testing assumes that the vehicles have already been built. Our virtual wind tunnel uses 'virtual vehicle' CAD models in a variety of acceptable formats obtained from most commercial finite element or surface modeling programs. Figure 1 shows the CAD representation we used for the Taurus. This model consisted of over 60,000 triangular elements. Vehicle preparation is the most time-consuming part of an analysis – sometimes taking 6 weeks for a finely detailed surface model! There is current work at Ford to find more efficient ways to build vehicle models with the fidelity we require, but this remains an open problem for industrious surface modelers.

Once a surface is provided, the engineer specifies zones where the volume mesh should be refined. PowerFlow uses a Cartesian computational mesh. Most cells are cubic in shape, except when a portion of the cell cuts through the body surface. In this case the cube is cut so that the actual surface of the body is captured correctly. Because we typically have a high density of cells near the body surface, there is very little, if any, loss of surface fidelity even in regions of high curvature.

In our analysis, three refinement zones were specified. Figure 2 illustrates the '120' region – a 'U' shaped volume that encloses the front-side glass and mirror on both sides of the car, as well as the wiper area. The 120 refers to the resolution level, and it means that this region will be filled with cubes (some whole, some cut as described earlier) whose dimension is 1/120th of the vehicle height, or 9·4 mm in this case. Two further, nested refinements were constructed
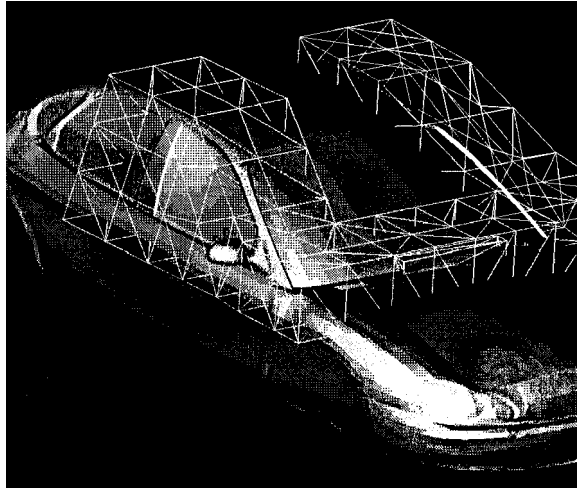
Figure 2. Taurus surface model showing the 120 region for mesh refinement.

with the finest surrounding the wiper blade (a 480 region with a mesh scale of 2·4 mm). This level was required to capture the details of the wiper assembly.

Figure 3 shows a close-up of the wiper region, detailing the wiper blade, leaf screen cavity, and side mirror. The wiper assembly shape reflects the fact that it is slightly compressed under tension, and that the blade is in contact with the windshield and follows its curvature. The blade itself is a triangular element that points normal to the windshield surface. The leaf-screen cavity retains all of the detail on an actual vehicle except for the air intake vents. The side mirror shroud and arm are exact, but the mirror region is flush at the end (*i.e.*, we did not recess the mirror itself into the shroud).

2.2. AUTOMESHING AND EXECUTION

At this stage we *automatically* generate the computational mesh needed for an analysis. On a 14-processor Sun E4000 workstation, a 6-million cell grid of the entire Taurus in the computational wind tunnel is generated in a few hours! This is a significant feat: with conventional CFD codes meshing the wiper assembly by hand alone would take considerable time and effort. The automeshing capability provided in this system renders this once-formidable task simple and quick.

2.3. THE COMPUTATIONAL WIND TUNNEL

Although the computational wind tunnel is physically much smaller than a real wind tunnel, it has a blockage ratio (frontal area of vehicle to inlet) of only 0·1%. In comparison, a 1/2 scale vehicle model in the Lockheed Low Speed Wind Tunnel provides what is called a low blockage environment with a ratio of 1·4%. Our tunnel has a ratio 1/14th thereof. Bottom line: there are no blockage effects in this computational wind tunnel, and hence no need to provide for any blockage corrections to body forces (drag, lift) computed there.

Figure 3. Close up of the Taurus windshield area.

2.3.1. *Test condition*

For our test case we simulated a speed of 70 mph. On the 14-processor E4000 we achieved an execution speed of 28,000 time steps/day (a single time step corresponds to 20 microseconds). With the first 2000 time steps ignored as startup effects, a snapshot of the flow field is output at every 4000 time steps, with the result being averaged over 4000 time steps, or 0·08 seconds. Of course, the length of the averaging period is up to the user, as is the amount of time attributed to startup effects. We compared, for example, the output at 4000 time steps to those at 8000, 12000, and 16000 to see if any appreciable changes on the side-glass pressures occurred and they did not.

2.3.2. *Wiper studies*

One problem that resulted in customer complaints on earlier Taurus models was referred to as 'water blow back' which occurred when wiper fluid is used to clean the window. At the end of the cleaning cycle with the wipers in the parked position, remaining fluid built up below the driver's side wiper, moved along it to the ends of the blade, and then proceeded up the windshield in two streak lines, one up the center of the windshield. It could also occur during a light rain when the wipers have a long time delay between wipes, thereby allowing water to build up below the blades. This phenomenon occurs because the wipers are located in the flow stream and recirculation regions form around them. We were interested, then, to see if our simulation could capture this.

Figure 4 illustrates how air flows around the wiper assembly by taking vertical slices through both wipers. Note that there are three recirculation regions. The first lies in the leaf-screen cavity and is set up as air flows over the hood lip. The remaining two regions are

Figure 4. Multiple streamline slices viewed from the passenger side.

positioned above and below the blade itself. We can see streamlines passing through various parts of the assembly, weaving their way in and around the arms and springs of the wiper assembly. The top image in Figure 5 shows the result of placing a linear streamline rake just at the tip of the Taurus wiper blade. From this we can see that the air direction is up the windshield.

The ability of our calculations to indicate the observed behavior for the Taurus was encouraging.[2] The water blow back problem was resolved by adjusting the lip of the hood in the cowl area so that the air stream flows over the wipers, allowing water to fall down from the blades, rather than up the windshield, as shown in the bottom two images of Figure 5 for two design variations.

2.3.3. *Wind-noise estimations*

As part of the validation process for the Wind Noise Modeller, driver's ear sound pressure level (SPL) measurements and side glass C_p pressure distributions were made on the Taurus at Lockheed. Both sets of data provided us with an excellent opportunity to correlate our

---

[2]The aerodynamic airflow over the hood, around the wipers, and along the windshield determines whether water would move up the windshield or not. Granted, a precise analysis would involve the effects of gravity on the liquid, the 'form' of the liquid (droplets or a big blob), the surface tension, the surface quality of the windshield (clean or dirty, wet or dry), etc. We only addressed the air flow directions. However, if the air velocity at the wipers was down into the cowl, then it is unlikely that liquid would go up. On the other hand, if the air velocity is up the windshield, it does not necessarily mean that liquid would also go up (but in the Taurus case it did). Thus, the airflow directions could be used to determine if water would flow down, and they would indicate favorable (though not necessarily sufficient) conditions for water to flow up.

Figure 5. Streamline rake at tip of the driver's side wiper blade (top: older Taurus model; bottom two: newer designs). Airflow is from right to left in all cases.

calculations to real-world measurements.

Side glass pressures. The compute pressure distribution on the side glass can be compared to that measured in the Lockheed wind tunnel. The experimental data, taken from 128 pressure taps on the window, can be used to construct a solid color image map of the C_p pressure distribution, shown in Figure 6.

Figure 7 shows the pressures computed with PowerFlow. We can see that, accounting for small differences in the color mapping and projection/perspective effects, we obtain a good agreement with the wind tunnel measurements. The 'hot spot' near the mirror arm is captured, as well as the mirror bubble region and A-pillar vortex (**Note**: the dotted line in figure 6 is the boundary of the window, whereas the solid line is the boundary of the pressure tap locations. Thus, the data is 'missing' a section of the A-pillar vortex region which is present in our computational picture).

3. Aeroacoustic analyses

We are now in a position to use this aerodynamic information to make a prediction on the sound level inside the passenger compartment due to wind noise. We take the C_p values from Figure 7 along with additional computational results and estimate the vortex size and aver-
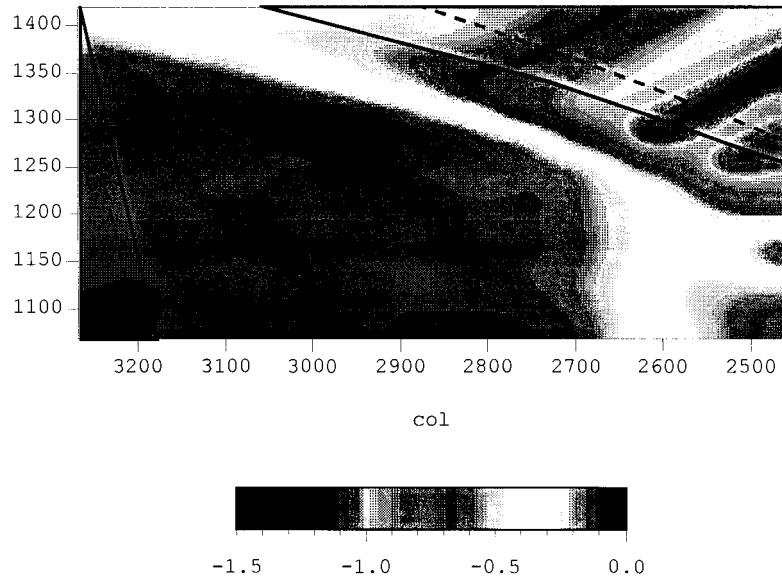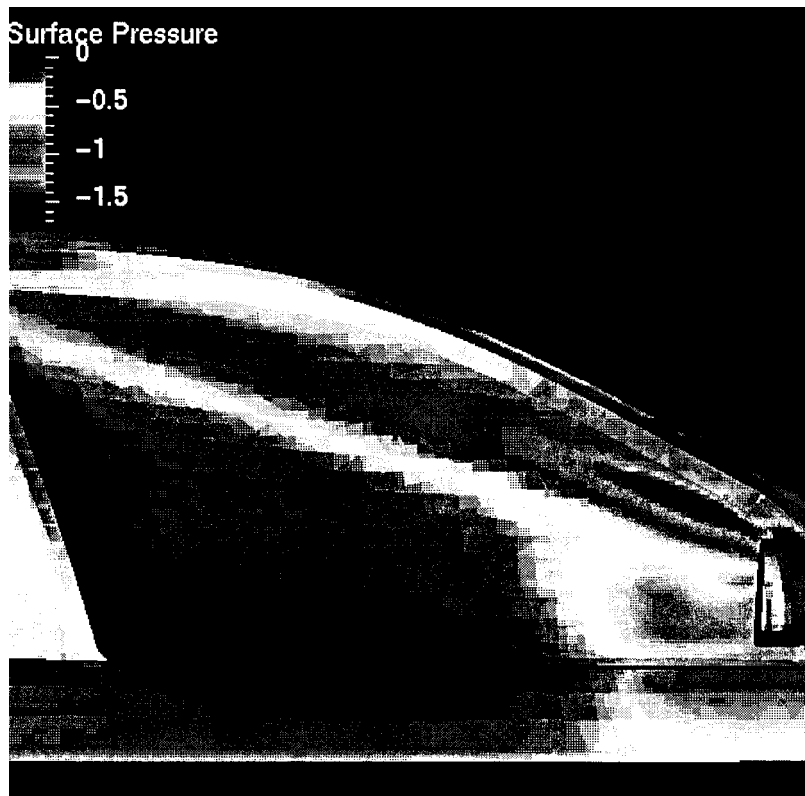
Figure 6. Wind tunnel Cp measurements.

Figure 7. Cp calculations from PowerFlow.

age C_p. A special graphics tool, *GrafPix*, has been developed to help automate this process. The engineer sketches the A-pillar and mirror bubble regions on-screen from an image like Figure 7 and the program automatically computes the fractional areas and average C_p values needed as input to the Wind Noise Modeller. Other parameters, like side-glass dimensions and thickness, door margins, and seal properties are measured on an actual vehicle. These are used in the next stage of our analysis: predicting the SPL at the driver's ear location using the Wind Noise Modeller.

3.1.   WIND-NOISE MODELLER – THEORY

3.1.1.   *Sound radiation from the side glass*
Sound pressure level (SPL) is usually defined as follows:

$$SPL = 10 \log_{10} \frac{<p^2>}{p_{\text{ref}}^2}$$

where $P_{\text{ref}} = 20 \ \mu\text{Pa}$ is the reference pressure. The mean-square pressure fluctuations can be related to the average sound power radiated by the structure using:

$$\langle p_0^2 \rangle = \frac{\rho c \Pi}{A_p}, \tag{1}$$

where

Π	– the average sound power radiated by the structure
ρ	– the density of air
c	– the speed of sound in air
A_p	– the area of the vibrating structure

The average sound power was given by Fahy [9, pp. 65]:

$$\Pi = \sigma \rho c A_p \langle v^2 \rangle, \tag{2}$$

where σ is the average radiation efficiency and $\langle v^2 \rangle$ is the mean-square vibrational velocity of the plate.

Radiation efficiency differs with plate-vibration modes, and depends on the way the plate is supported. Statistical Energy Analysis (SEA) predicts that support is only important near the fundamental frequency f_{11};[3] experiments (see for example [4]) show that sound power varies little between simply supported and clamped plates. We therefore use an empirical expression for the average radiation efficiency of a simply supported plate, in a form similar to that presented by Beranek [2, pp. 275-278, 362-364]:

$$\sigma = \begin{cases} \dfrac{Pc}{\pi^2 A_p f_c} \sqrt{f/f_c} & \text{for } f < f_c/4 \\[2ex] \dfrac{P\lambda_c}{A_p} g(\alpha) & \text{for } f_c/4 < f < f_c \\[2ex] 1 & \text{for } f > f_c \end{cases}$$

---

[3] $f_{11} = (L_1/L_2 + L_2/L_1) \, c^2 / 4A_p f_c$. For a 'typical' side glass this frequency is around 80 Hz.
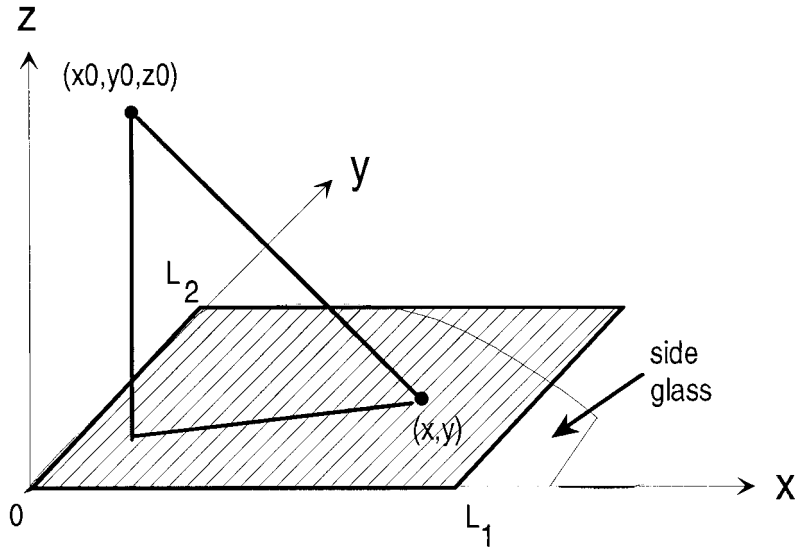
Figure 8. Radiation of sound diagram. Plot shows side glass along with the rectangular plate representing it (plate has equal surface area).

where P is the perimeter of the plate, f_c is the acoustical coincidence frequency, and

$$\alpha = \sqrt{f/f_c}\lambda_c = c/f_c$$

$$g(\alpha) = \frac{1}{4\pi}\left[\frac{(1 - \alpha^2)\log\left(\dfrac{1+\alpha}{1-\alpha}\right) + 2\alpha}{(1 - \alpha^2)^{1\cdot5}}\right]$$

Equation 1 gives us the SPL near the glass surface, but we are interested in the value at the driver's ear position. Noting that $\Pi/A_p = I_0$ is the average intensity of sound waves near the surface of the plate, we can express the mean-square pressure fluctuations at the driver's ear position as,

$$\langle p^2 \rangle_{\text{ear}} = \rho c I, \tag{3}$$

where I is the average intensity of sound waves at the ear position.

Let us consider a simply supported plate characterized by its length L_1 and width L_2, a uniform mass per unit area m_s, and flexural rigidity $D = \frac{Eh^3}{12(1-\gamma^2)}$, where E is the Young's modulus of the glass, h the plate thickness, and γ the Poisson coefficient. If we assume that I_0 is uniform on the plate and that it radiates hemispherically, we can express the value of I at some point (x_0, y_0, z_0) (see Figure 8) as,

$$\zeta = \frac{I}{I_0} = \frac{1}{2\pi}\iint\limits_{A_p} \frac{z_0 \mathrm{d}x\mathrm{d}y}{\left((x - x_0)^2 + (y - y_0)^2 + z_0^2\right)^{3/2}} \tag{4}$$

where the double integral, evaluated over the surface of the plate, can be evaluated numerically and, in some cases, analytically. ζ is the attenuation factor that accounts for the ear position relative to the plate.

If we choose $x_0 = 0$ and $y_0 = L_2/2$, which is a reasonable choice of the driver's ear position (*i.e.*, the driver's ear is along the B-pillar and halfway up the glass), we obtain

$$\zeta = \frac{1}{\pi} \arctan \left(\frac{L_1 L_2}{z_0 \sqrt{4z_0^2 + 4L_1^2 + L_2^2}} \right), \tag{5}$$

where L_1 and L_2 are the length and the width (or height) of the plate, respectively,[4] and the plate area $A_p = L_1^* L_2$. Let z_0 represent the average normal distance from the ear to the glass surface. Combining Equations (2–4) we finally obtain:

$$\langle p^2 \rangle_{\text{ear}} = \sigma \rho^2 c^2 \langle v^2 \rangle \zeta.$$

To complete our analysis of the sound radiated by the side glass we need to estimate the mean-square vibration velocity term in the above expression. This is complicated by the fact that on a typical side glass there are three flow regimes present: a vortex flow induced by the airflow over the A-pillar and the side mirror, a fully-established turbulent boundary-layer flow, and a transitional regime (reattaching flow) between them. One might consider the side glass flow as a combination of these three basic flow patterns. The mean-square vibrational velocity term is proportional to the wavenumber-frequency pressure spectra for each type of flow regime (see [3, pp. 529–560], [5], [6], [8, pp. 286–294] for more details). Strictly speaking, we need to perform a complex analysis of the plate vibration for each if we want to combine different flow patterns. However, in SEA this restriction may be neglected and flow regions can be considered separately. In such cases, only the spatial averaging of flexural bending modes will change. *i.e.*, each mode will be averaged not over the entire plate surface but only over the area that is covered by a particular type of flow. This leads to the power input from a particular flow regime being proportional to the area of the plate under this flow. Thus the different wavenumber-frequency spectra enter with their weights:

$$\varphi_i = \frac{\text{area}_{\text{flow}}}{\text{area}_{\text{plate}}}$$

This leads us to

$$\langle v^2(\omega_f, \Delta\omega_f) \rangle = \frac{\pi^2 \Delta\omega_f}{m_s^2 \eta \kappa c_l \omega_f} \left\{ \varphi_v \Phi_v + \varphi_r \Phi_r + \varphi_t \Phi_t \right\}, \tag{6}$$

at center frequency ω_f and band width $\Delta\omega_f$. Here the subscripts v, r, and t stand for vortex, reattaching, and turbulent boundary layer, respectively. The glass loss factor is η, κ is the radius of gyration, and c_l is the longitudinal wave speed. Since the glass is subdivided into only these three flow regimes we have

$$\varphi_v + \varphi_r + \varphi_t = 1.$$

Equation 6 is our final expression since, with it, we can model any combination of flows. Combining this with our earlier expressions enables us to compute the SPL at, say, the 1/3 octave frequencies if we can provide expressions for the frequency spectra of each flow regime. These are obtained through experiments (see [10–17] for spectral forms for the different flow regimes). The net result is quite significant; we can produce noise estimates (an Inherently non-steady quantity) using only steady-state computations!

---

[4] The width L_2 is set equal to the height of the side glass. The length L_1 is set to what it needs to be so that the area of the resulting rectangular plate equals the area of the side glass.
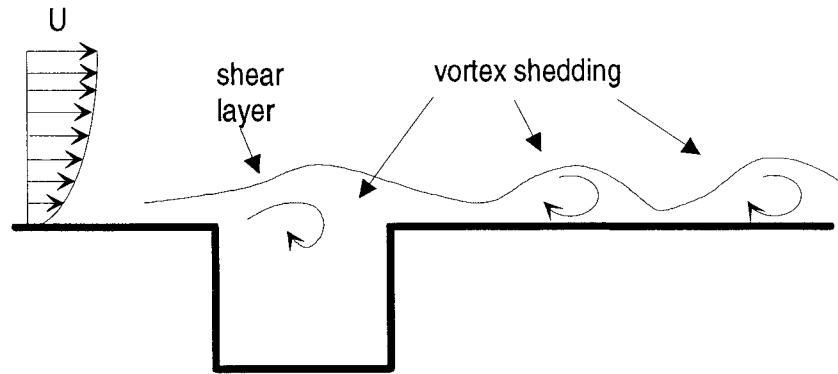
Figure 9. Schematic of flow over door gap showing vortex shedding and impingement.

3.1.2. *Seal effects*

So far we have concentrated on the noise radiated from the vibrating side glass alone. The resulting SPL is only appropriate for a taped vehicle. We therefore also need to examine the amount of noise transmitted through the door seals. There are two mechanisms for noise transmission. The first is when the seals lift off the door or body frame and permit air to escape from the passenger compartment. This is called *aspiration* and is not so much transmission *through* a seal as it is *past* it. It is quite common at high speeds and high yaw angle for a vehicle with only one seal (*e.g.*, the door weatherstrip). It also occurs around poorly designed glass runs, particularly along the upper edge of the window. This is not handled by the Wind Noise Modeller or treated in our analysis.

The second mechanism occurs when the seal remains in contact with the vehicle surface but vibrates due to pressure fluctuations in the door gaps. Since the fluctuations are aerodynamics in nature, we can use experimental data to help predict at which critical frequencies we can expect noise transmission. Let us begin with the one at which most seal noise is transmitted.

Flow over door gap margin. The first, and most significant, critical frequency occurs due to flow over the door gap. This is illustrated in Figure 9 below. Numerous experiments on turbulent flows over rectangular channels have revealed the critical shedding frequency f_n as a function of channel geometry, boundary-layer thickness and free-stream flow speed. This can be summarized by the following formula:

$$f_n = 0.33(n - 0.25)U / L,$$

where L is the length of the channel (related to the door margin), U the local speed and n the number of vortices across the channel. Typically, for door margins as small as ours (on the order of 5–8 mm) $n = 1$. We expect that sound will be transmitted through the seals at this frequency. Since the shedding process is unstable, we do not expect that *only* this frequency will emit sound and so we have made the heuristic assumption that noise will be transmitted in the form of a Gaussian distribution centered about this critical frequency. The amplitude and spread of the Gaussian are determined by engineering judgment based on experimental data over a wide range of vehicles.

Noise transmission through the seals. In addition to the critical shedding frequency, there are those associated with the locations of zero transmission loss (TL) for the seal system.
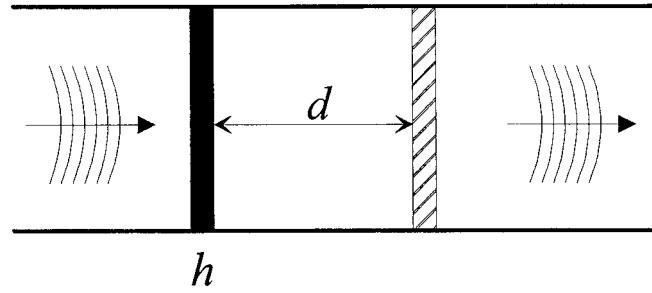
Figure 10. Schematic of noise transmission through a two-wall system.

Consider the following arrangement: where h is the seal wall thickness, ρ the seal density, and d the separation distance between the two walls of the seal (this is an idealization of a single 'circular' seal; the rest of the seal wall lies along the upper and lower surfaces in the above diagram). A sound is generated on the left of the channel and we want to know the nature of the sound that will emit on the right. One can show that zero sound transmission loss (sound passing through without attenuation) occurs at the critical frequency ω that satisfies the nonlinear equation:

$$1 = \left(1 + \frac{\beta^2}{4}\right)^2 + \frac{\beta^4}{16} - \frac{\beta^2}{2}\left(\frac{\beta^2}{4} + 1\right)\cos\left(\frac{2\omega d}{c} - \alpha\right),$$

where

$$\sin\alpha = \frac{4\beta}{\beta^2 + 4} \quad \text{and} \quad \beta = \frac{\omega\rho h}{\rho_0 c}.$$

This equation looks more formidable than it actually is since we observe that the equality will be satisfied when the cosine term equals one, or when

$$\left(a^2\omega + \frac{4}{\omega}\right)\sin(\omega b) - 4a = 0,$$

where

$$a = \frac{\rho h}{\rho_0 c} \quad \text{and} \quad b = \frac{2d}{c}.$$

There is only one frequency that satisfies the above relationship and it can be determined numerically. It is a function of the seal geometry and material properties. If we further assume that ωb is small, the above equation can be approximated by

$$\left(a^2\omega + \frac{4}{\omega}\right)\left(\omega b - \frac{\omega^3 b^3}{6}\right) - 4a = 0,$$

from which we obtain a biquadratic equation that can be solved exactly giving

$$f_{TL} \equiv \frac{\omega}{2\pi} = \frac{1}{2\pi}\sqrt{\frac{-a_2 - \sqrt{a_2^2 - 4a_1 a_3}}{2a_1}},$$

$$a_1 = \frac{a^2 b^3}{6}, \quad a_2 = \left(\frac{2b^3}{3} - a^2 b\right) \quad \text{and} \quad a_3 = 4(a - b).$$

Now the result we just presented is valid for a two-wall seal system, *i.e.*, for a single seal like the door weatherstrip. What if there are additional seals? We can still obtain the critical frequencies, albeit by a more involved numerical procedure (there are $(n-1)$ such frequencies for an n-wall system). However, if we assume that in adding seal walls the separation distance, wall thickness, and material properties remain constant, then we can determine the frequencies for the n-wall case with just the two-wall value. This can be summarized in the following table:

Table 1. Scale factors for a 2, 3, 4 and 5-wall system.

NUMBER OF WALLS:	MULTIPLICATIVE FACTOR:
2	1
3	0·71 and 1·24
4	0·54, 1 and 1·31
5	0·44, 0·83, 1·15 and 1·35

We can obtain the critical frequencies for any number of walls by multiplying f_{TL} given above by the appropriate factors in the table. For example, if the critical frequency for a two-wall system is 800 Hz, then a four-wall system would have three critical frequencies at 432 Hz (800 times 0·54), 800 Hz and 1048 Hz (800 times 1·31).

The resultant SPL that the Wind Noise Modeller generates is a combination of the noise from the vibrating side glass and the noise transmitted by the door seals.

3.2. HOW WELL DOES THE WNM PREDICT SPL?

Figure 11 illustrates how well the VAWT system works on our Taurus example. We start with the calculations. The surface Cp distribution is computed using the PowerFlow CFD code and *GrafPix* is used to extract the relevant information. The Wind Noise Modeller is then used as described above to predict the sound pressure levels (SPL) at the driver's ear (solid blue line). This compares very favorably with actual SPL measurements (yellow square markers) from wind tunnel tests at Lockheed. If fact, we routinely come to within 3 dB of the experimental values across the entire spectrum. (This is significant because most people have difficulty distinguishing sounds that differ by less than 3 dB.) We can then evaluate design variations on this vehicle. A new shape is run through the VAWT yielding a new side-glass Cp distribution that, in turn, is fed to the WNM and compared against the previous calculation. The result is a predicted drop in interior sound level of 1·9 dB. Actual measurements indicated a 1·7 dB drop! This is significantly more accurate than previous attempts at predicting interior wind noise ([18–20]).

3.3. VIRTUAL ACOUSTICS

To provide the engineer with a virtual acoustics capability, the SPL spectrum computed by the WNM can be compared to the experimental data by playing both through a set of speakers on a PC. DSP boards take a white noise sound signal as input and 'shape' it to the particular spectrum being analyzed. While this sound is not precisely the same as the actual wind noise, it does allow us to evaluate the difference and direction between two sets of data. The engineer can toggle between three different sounds: the experimental data, the predicted spectrum for the current design, and a saved spectrum from a previous design.
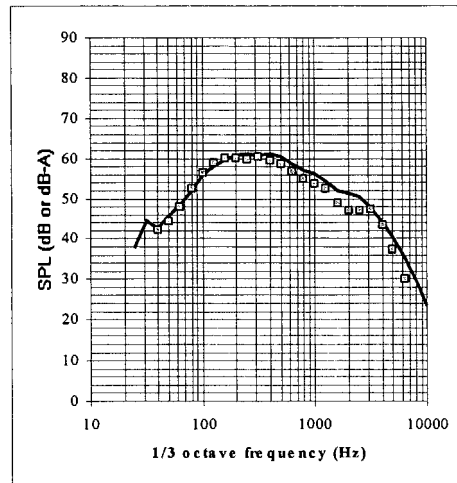
Figure 11. Comparison of predicted SPL (blue line) with measured values (yellow squares)

4. Concluding remarks

We have developed a virtual aerodynamic/aeroacoustic wind tunnel. It starts with a CAD representation of a vehicle and renders an aerodynamic evaluation quickly and efficiently on a deskside workstation with a minimum amount of user intervention. The steady-state surface pressures on the front-side glass are computed by use of a novel CFD approach that uses a lattice gas method to represent the fluid motion. In this model, particles move on a three-dimensional Cartesian lattice and collide under rules that satisfy conservation-of-mass and momentum laws. These collisions, and their resulting advection to neighboring nodes on the lattice, result in fluid-dynamic behavior without having to solve the standard Navier-Stokes equations for fluid mechanics. This information is then fed to the Wind-Noise Modeller for a prediction of interior sound levels. The modeler uses a statistical energy approach to compute the sound inside the vehicle at the driver's ear location by combining the pressure information from the CFD analysis with experimental results for a variety of flow types. The sound from the side-glass vibration is then combined in the modeler with the noise generated by the door seals to yield a total sound that the driver hears as wind noise. This sound can finally be played through speakers for an analysis of alternate vehicle designs. This is a major advancement in computer-aided engineering capability that should result in our producing quieter, more customer-satisfying vehicles with less engineering cost and effort.

The greatest challenge still to be overcome is the rapid development of alternate CAD models representing design changes. The VAWT could be used most effectively in a Design-of-Experiments statistical approach if the CAD models could be created quickly. This would require the ability to modify dynamically the surface under certain mathematical constraints, while still retaining the design intent. How to do this effectively remains an open problem.

References

1.   G.S. Strumolo, The wind noise modeller. *Society of Automotive Engineers* (1997) paper #97–1921.
2.   L.L. Beranek, *Noise and Vibration Control*. New York: McGraw-Hill (1971) 804pp.
3.   W.K. Blake, *Mechanics of Flow-Induced Sound and Vibration*. Orlando: Academic Press (1986) 974pp.

4. J.R. Callister and A.R. George, The transmission of aerodynamically-generated noise through panels in automobiles. *Second International Congress on Recent Developments in Air- and Structure-Borne Sound and Vibration* Auburn University (1992)

5. D.M. Chase, Modelling the wavevector-frequency spectrum of turbulent boundary layer wall pressure. *J. Sound Vibr.* 70 (1980) 29–67.

6. G.M. Corcos, The structure of the turbulent pressure field in boundary-layer flows. *J. Fluid Mech.* 18 (1964) 353–378.

7. H. Cramer and M. Leadbetter, *Stationary and Related Stochastic Processes*. New York: Wiley (1967)

8. L. Cremer and M. Heckl, *Structure-Borne Sound: Structural Vibrations and Sound Radiation at Audio Frequencies*. Berlin: Springer-Verlag (1988) 528pp.

9. F. Fahy, *Sound and Structural Vibration: Radiation, Transmission, and Response*. Orlando: Academic Press (1985) 309pp.

10. T.M. Farabee and M.J. Casarella, Measurements of fluctuating wall pressure for separated/reattached boundary layer flows. *ASME Winter Annual Meeting*, Miami Beach, Florida, (1985)

11. T.M. Farabee, An experimental investigation of wall pressure fluctuations beneath non-equilibrium turbulent flows. Maryland: PhD Dissertation, David W. Taylor Naval Ship Research and Development Center (1986)

12. F.R. Fricke, Pressure fluctuations in separated flows. *J. Sound Vibr.* 17 (1971) 113–124.

13. F.R. Fricke and D.C. Stevenson, Pressure fluctuations in a separated flow region. *J. Acoust. Soc. America* 44 (1968) 1189–1968.

14. M. Gad-el-Hak and R. Blackwelder, The discrete vortices from a delta wing. *AIAA J.* 23 (1985) 961–962.

15. A.M. Mohsen, Experimental investigation of the wall pressure fluctuations in subsonic separated flows, Boeing Company Report No. D6-17094 (1968)

16. J.M. Witting, A spectral model of pressure fluctuations at a rigid wall bounding an incompressible fluid, based on turbulent structures in the boundary layer. *Noise Control Eng. J.* 26 (1986) 28–43.

17. W.E. Zorumski, Classic theoretical approaches to computational aeroacoustics. In: J. Hardin & M.Y. Hussaini (eds.), *Computational Aeroacoustics* Berlin: Springer-Verlag (1992) pp.41–49.

18. M. Watanabe, M. Harita and E. Hayashi, The effect of body shape on wind noise. *Soc. Automotive Engrs.* (1978) paper #78-0266.

19. S. Haruna, T. Nouzawa, I. Kamimoto and H. Sato, An experimental analysis and estimation of aerodynamic noise using a production vehicle. *Soc. Automotive Engrs.* (1990) paper #90-0316.

20. A.R. George, Automobile aerodynamic noise. *Soc. Automotive Engrs.* (1990) paper #90-0315.